Research Article | Vol. 12, No. 10 / 1 Oct 2021 / Biomedical Optics Express 6013
Biomedical Optics EXPRESS

Optical neural stimulation using the thermoplasmonic effect of gold nano-hexagon

HASSAN TAJARENEJAD, MOHAMMAD ALI ANSARI,* SOHEILA AKBARI, HANIEH YAZDANFAR, AND SEYEDEH MEHRI HAMIDI

Laser and Plasma Research Institute, Shahid Beheshti University, Tehran 1983969411, Iran
**m_ansari@sbu.ac.ir*

Abstract: The use of nanoparticle photothermal effect as adjuvants in neuromodulation has recently received much attention, with many open questions about new nanostructures' effect on the action potential. The photothermal properties of hexagonal gold nanoparticles are investigated in this work, including the absorption peak wavelength and light-heat conversion rate, using both experimental and simulation methods. Furthermore, the ability to use these nanostructures in axonal neural stimulation and cardiac stimulation by measuring temperature changes of gold nano-hexagons under 532 nm laser irradiation is studied. In addition, their thermal effect on neural responses is investigated by modeling small-diameter unmyelinated axons and heart pacemaker cells. The results show that the increase in temperature caused by these nano-hexagons can successfully stimulate the small diameter axon and produce an action potential. Experiments have also demonstrated that the heat created by gold nano-hexagons affects toad cardiac rhythm and increases T wave amplitude. An increase in T wave amplitude on toad heart rhythm shows the thermal effect of nano hexagons heat on heart pacemaker cells and intracellular ion flows. This work demonstrates the feasibility of utilizing these nanostructures to create portable and compact medical devices, such as optical pacemakers or cardiac stimulation.

1. Introduction

Plasmonic nanoparticles (NPs) are absorbing from the fundamental science point of view as well as in applications such as optics, medicine, clinical diagnosis, and therapy due to their localized surface plasmon resonances (LSPRs)[1–3]. The properties of LSPR include resonance wavelength and spectral range, which vary depending on the shape, such as nanospheres, nanorods, nanobars, nanostars, nanoprisms, nanocrystals, and the size of the plasmonic NPs [4–6]. Among these different shapes, nanostars have displayed extraordinary properties and highly enhanced electromagnetic fields with promising applications in biosensing, bioimaging, and biodetection [7,8]. To guarantee these NPs in the biomedical area, intensifying local electric fields is used, especially around their tips and sharp corners [9,10] and red shifting in the resonance answer by adjusting the size of particles and corners.

Various neurological disorders such as Parkinson's disease, hearing loss, and heart arrhythmia are common diseases globally controllable by neural stimulation. In the last decade, infrared neural stimulation (INS) has shown significant potential for neural modulation [11–14]. In addition, optical methods can be considered as an alternative way for electrical heart pacemakers. Infrared radiation (IR) has been shown to raise heart rate in embryonic quail [15], rabbits [16], and rats [17]. Cause primary underlying mechanism of infrared neural stimulation is based on thermal effects, so nano heaters can be helpful for enhancing the photothermal effect. During INS, the photothermal effect of gold nanorods was demonstrated to increase neural activity in cells and nerves [18–21]. Carbon nanoparticles have also been shown to enhance the INS of the sciatic nerve [22]. In addition, a two-dimensional structure based on gold nanorods helps us benefit from INS for regulating membrane depolarization [23].

#438593 https://doi.org/10.1364/BOE.438593
Journal © 2021 Received 27 Jul 2021; revised 23 Aug 2021; accepted 26 Aug 2021; published 7 Sep 2021

Biomedical Optics EXPRESS

In all these procedures, neural stimulation by plasmonic nano heaters' physical phenomena has not been clearly explained. As a result, gold nano-hexagons (AuNHs), a novel type of nanoparticle, are employed in the proximity of neurons to simulate their effect in this medium, making these nano heaters more sensitive to neural stimulation. First, AuNHs' photothermal effects, temperature behavior, and heat diffusion in the cellular environment are studied. Then, according to these results, the possibility of using these nanoparticles in axonal neural stimulation was evaluated. Finally, the effects of heating on cardiac action potential were simulated. The results are evaluated by an animal study wherein the increase in temperature by AuNHs under 532 nm irradiation on the toad heart area was studied. These results show the potential of AuNHs as an effective structure on axonal and cardiac tissues. According to recent developments in the compact platform design for neural stimulation [24,25], this study could be considered an early stage study to design portable optical heart pacemakers based on nanoparticles.

2. Material and methods

2.1. Synthesis of gold nano-hexagons

In the fabrication of AuNHs, Cetyl trimethylammonium bromide (CTAB), Tetrachloroauric acid ($HAuCl_4$), Sodium hydroxide (NaOH), ascorbic acid (C_6H_8O), silver nitrate ($AgNO_3$), and acetone (C_3H_6O) were used. The synthesis method followed in this project was the same as the protocol used by Trigari et al. [26–28]. The synthesis of AuNHs is based on the reduction of $HAuCl_4$. AuNHs preparation was started by making a 3 mL solution of CTAB (50mM) and $HAuCl_4$ (2mM) mixture in water. The color of this solution was dark yellow. Afterward, 80 µL of NaOH (0.25 M) and 200 µL of ascorbic acid (40 mM) were added to the solution. By adding NaOH and ascorbic acid, the solution became colorless. In the last steps of the synthesis, 60 µL of $AgNO_3$ (10 mM) and 65 µL acetone were added to the solution. All the solutions were prepared in HPLC water. The solution containing NHs was kept at 25°C overnight to complete the reduction of AuNHs.

2.2. Neural activity simulation

2.2.1. Axonal action potential

An unmyelinated axon with a diameter of 5µm was modeled using the modified Hodgkin-Huxley model. In the original Hodgkin-Huxley (H-H) model, the membrane capacitance is constant. However, H-H equations were rewritten based on temperature-dependent capacitance to describe the increase in axon's temperature due to nanostructures generated heat. Based on presented results in [29], the relation between membrane capacitance and temperature is defined as follows based on Curie–Weiss law:

$$C_m = c_o + \frac{k}{\delta T}\ , \tag{1}$$

where δT is defined in this as follows:

$$\delta T = T_c - T, \tag{2}$$

wherein $k = 2.2\frac{\mu F}{cm^2}$, $c_o = 0.8\frac{\mu F}{cm^2}$°C and T_c=31°C according to Ref. [30]. Thus, temperature changes over time for short pulses can be defined as follows [31]:

$$T = \Delta T \gamma t \qquad t < t_{pulse}. \tag{3.a}$$

$$T = \Delta T \beta \{\varphi e^{-n_1 t} + (1-\varphi)e^{-n_2 t}\} \quad t > t_{pulse}. \tag{3.b}$$

ΔT denotes the amount of the temperature changes and constant parameters $n_1 = 0.015$, $n_2 = 0.03$, and $\varphi = 0.454$. The parameters γ and β are also numbers between 0 and 1 that change

Biomedical Optics EXPRESS

with temperature changes. The total currents through the membrane (based on the H-H model) are defined as follows:

$$I = C_m\left(\frac{dV}{dt}\right) + I_k + I_{Na} + I_l + I_H. \tag{4}$$

Wherein ionic currents are sodium, potassium, leakage currents. Effect of the heat of nanoparticles under irradiation on membrane capacity is considered as I_H.

2.2.2. Cardiac action potential

The behavior of Purkinje fibers under thermal stimulation was studied to simulate the variation of cardiac action potentials. For this purpose, Hodgkin-Hoxley based equations from Ref. [32] were used.

$$I = C_m\left(\frac{dV}{dt}\right) + I_{Na} + I_{K1} + I_{K2} + I_{Cl}. \tag{5}$$

That there are sodium and chloride currents and two types of potassium currents.

In this study, the neural models were simulated by NEURON software [33]. All parameters employed in the simulation are shown in Table 1 and Table 2 in the Appendix section.

2.3. Photothermal effect simulation

The pyGDM tool kit was used to calculate the total heat generated inside the nanostructure. pyGDM is based on the Green dyadic method (GDM) and calculates the total field E(r,ω), inside a nanostructure [34]:

$$E(r,\omega) = E_0(r,\omega) + \sum_{j=1}^{N} G(r_i, r_j, \omega).\chi_e(r_j,\omega).E(r_j,\omega)V_{cell}. \tag{6}$$

Where $E_0(r,\omega)$ is the electric field of the incident light, $G(r_i, r_j, \omega)$ is a tensor describing the environment that nanostructure is located inside that, and $\chi_e(r_j,\omega)$ is the dielectric function of nanostructure material. The total electric field inside the nanostructure is calculated using meshing nanostructure in cubic sections. Where $V_{cell} = d^3$ is the volume of every single mesh with the height of d. When a nanostructure is irradiated, a part of the light is scattered, and the other part is absorbed. The absorbed part eventually turns into heat. The total heat generated inside the nanostructure is given by:

$$Q(\omega) = \int_V q(r,\omega)dr = \frac{\omega}{8\pi}\int_V \acute{\epsilon}(r)|E(r,\omega)|^2 dr. \tag{7}$$

Where $q(r,\omega)$ is the volumetric power density of heat generation and $\acute{\epsilon}(r)$ is the imaginary part of permittivity of nanostructure material. The temporal change in temperature of axons adjacent to nanoparticles may therefore be estimated as follows:

$$\frac{\partial T}{\partial t} = \frac{k}{\rho c_p}\frac{\partial^2 T}{\partial x^2} + \frac{Q_V}{\rho c_p}, \tag{8}$$

where T is temperature change and Q_V is volumetric heat generated by nanoparticles. Aqueous environment parameters were used to calculate heat diffusion because 60% to 90% of neural cells are composed of water [35]. $k = 0.6\ \frac{W}{m.k}$ is thermal conductivity, $c_p = 4182\ \frac{j}{k.kg}$ is specific heat and $\rho = 997\frac{kg}{m^3}$ is the density of water.

Biomedical Optics EXPRESS

2.4. AuNHs temperature change experiment

A continuous 532 nm laser (53220, Mahfanavar, Iran) was used to illuminate AuNHs. The laser was set at a distance of 5 cm from the top of the AuNHs. The laser beam diameter is 3 mm, and its power density is $80\frac{mW}{cm^2}$. The temperature was measured by a thermocouple (TM-916, LUTRON electronic enterprise co, Taiwan). All experiments are performed four times a week to ensure the stability of temperature changes of AuNHs.

3. Results and discussion

TEM images for AuNHs samples were recorded a week after fabrication for the sample with 80 µL of NaOH and sample without NaOH, as shown in Fig. 1(A).

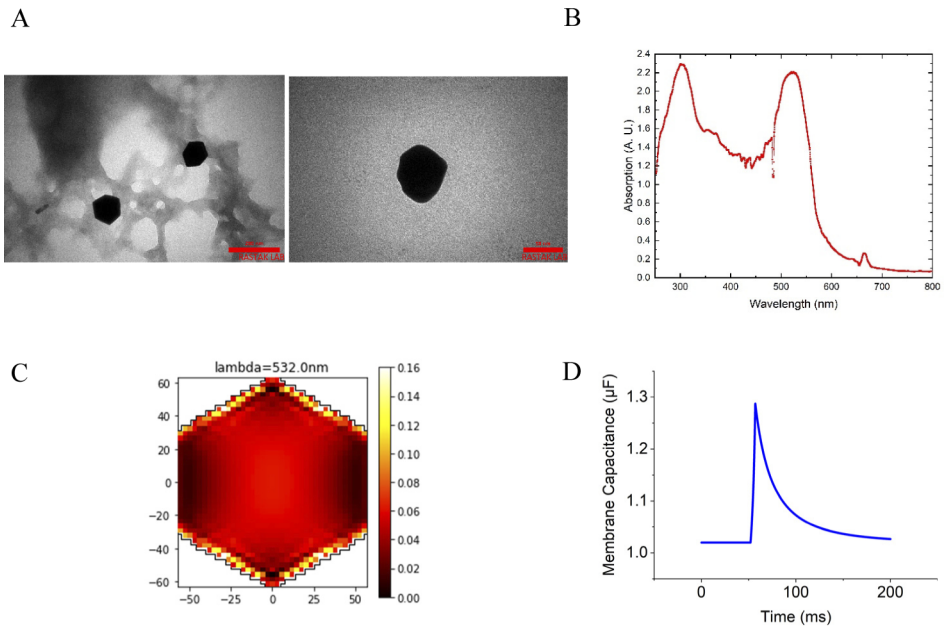

Fig. 1. **(A)** TEM images of AuNHs taken a week after fabrication. **(B)** The absorption spectrum of AuNHs. **(C)** The geometry of a single AuNH discretized on a cubic lattice and the heat distribution($\frac{nW}{\mu m^2}$) simulated within it. **(D)** Change in membrane capacitance under 5 ms heat generated by AuNHs with a 5.5°C increase in temperature of the axon. Membrane capacitance increases by About 0.3 µF.

Figure 1(B) shows the absorption spectrum of AuNHs. The prominent peak at 530 nm belongs to the Au absorption, and the shoulders appear due to the sharp corners of the polygonal. In addition, the heat distribution was calculated, and as can be seen in Fig. 1(C) in gold hexagonal nanoparticles, significant heat was generated at the corners of the structure. Temperature increases of up to 6°C were seen after 20 minutes of irradiation, as illustrated in Fig. 2(A). The temperature increased with a steep slope in the first 6 minutes of irradiation at a rate of $0.86\frac{^\circ C}{min}$. The AuNHs also lost heat with a slope of $0.91\frac{^\circ C}{min}$ in around 4 minutes after the laser radiation was turned off. The experiment is carried out at a temperature of around 23 °C in the laboratory.

3.1. Heat generation and distribution of AuNHs

The first one requires predicting the appropriate wavelength for heating the nanoparticles used in this study. The suitable wavelength can be computed by using Eq. (7). Figure 2(B) depicts

Biomedical Optics EXPRESS

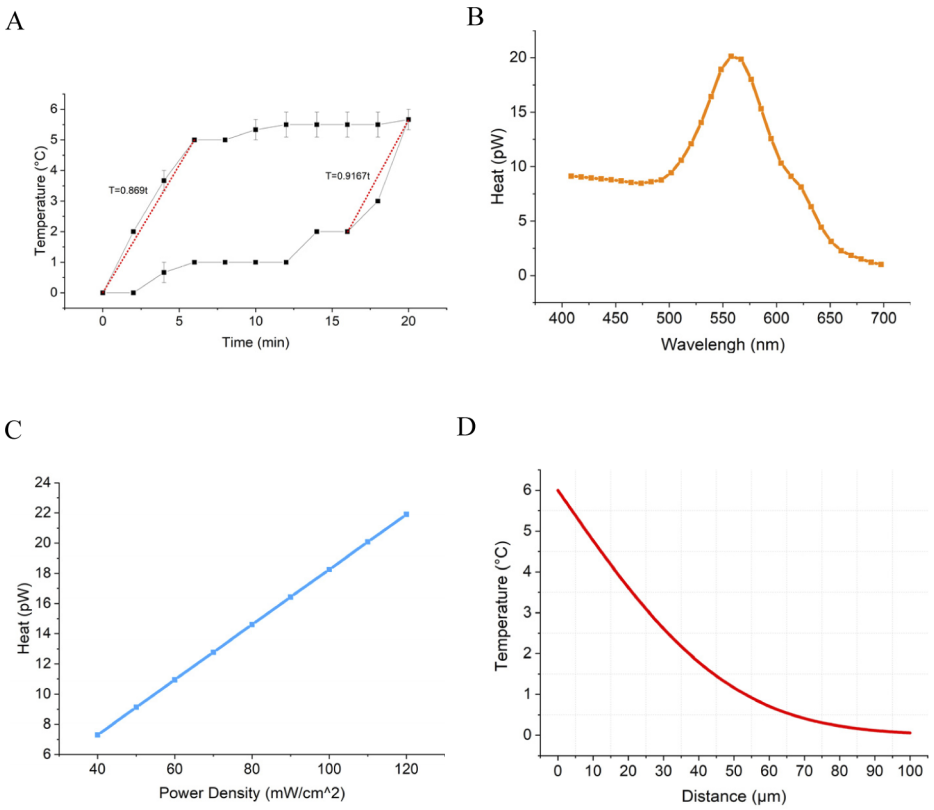

Fig. 2. **(A)** Temperature hysteresis diagram of AuNHs. A considerable rise occurred within the first 6 minutes after starting the irradiation at a rate of $0.86\frac{^{\circ}C}{min}$. Also, after the laser radiation was turned off, AuNHs temperature decreased at a rate of $0.91\frac{^{\circ}C}{min}$ **(B)** The influence of wavelength on single AuNH heat generation. **(C)** Heat generation inside the AuNH via radiation with a wavelength of 532 nm. With a power density of $80\frac{mW}{cm^2}$ roughly15 pW heat inside the nanostructure was generated (Variation of for different versus power density). **(D)** Temperature variations in distances near nanoparticles in the watery environment after 5 ms putting beside AuNHs.

the spectral heating of these nanoparticles. As shown in this figure, the best wavelength for photothermal conversion is about 550 nm. It is compatible with the absorption spectrum of the AuNHs, as shown in Fig. 1(B). Then heat generation inside a single AuNH for different laser power densities (lambda of 532 nm) was calculated as depicted in Fig. 2(C). Finally, based on the maximum observed temperature rise of 6° C in the experiment, the heat diffusion equation was used to estimate the radial distribution of temperature around the nanoparticles, as shown in Fig. 2(D). Figure 2(D) shows that temperature significantly decreases at a distance of 100 μm around AuNHs. Heat transfer in 5 ms was calculated considering the importance of thermal gradient for neural stimulation.

Assuming heated AuNHs are located in a neural environment to calculate the temperature rise in AuNHs surroundings. The one-dimensional heat diffusion equation is solved up to a distance of 200 μm from the AuNHs. Water's thermal conductivity and thermal diffusivity were used because the cell environment is composited mainly by water. As shown in Fig. 2(D), a significant increase in temperature can be seen at a distance of around 20 μm from AuNHs. It means axons with a diameter of up to 20 μm could be significantly affected by the thermal effects of AuNHs.

Biomedical Optics EXPRESS

3.2. Axonal neural stimulation

An unmyelinated axon with a diameter of 5 µm was modeled to investigate the potential of nerve stimulation with heating as well as the behavior of neural responses. A temperature-dependent Hodgkin-Huxley model was defined for this axon. According to the temperature variations observed in the experimental and simulation results, placing the axon next to the nanoparticles for 5 ms induced about 6 °C increase in temperature to the modeled axon. Figure 3(A) shows that action potential was generated with a 6°C increase in axon temperature, and the axon was successfully stimulated.

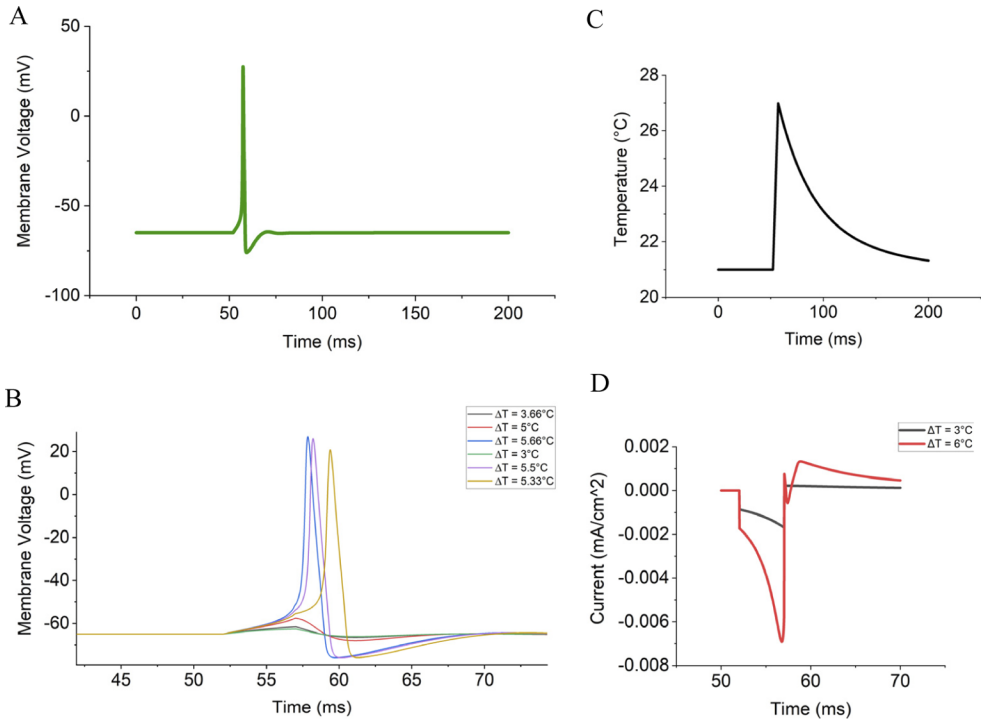

Fig. 3. **(A)** An action potential generated by an increase of 6°C in temperature during 5 ms. **(B)** A linear increase in temperature in 5 ms. **(C)** Membrane voltage changes of axon due to increased temperature in range 3 to 5.66°C. Temperature increase under 5.33°C could not stimulate the axon. **(D)** Induced Current through the membrane, produced by 3°C and 6°C increase in temperature.

By repeating the experiment for temperature increase between 3 to 6 ° C, it was observed that to generate AP in the axon, it is required to increase the temperature at least about 5.3 ° C. This corresponding to other nanostructures like gold nanorods that have been reported to have led to successful neural stimulation in temperature increasing range under 10 °C [18,21]. As shown in Fig. 3(B), a 5 ° C increase in temperature could not stimulate the axon. Because the temperature drops as the distance from the AuNHs increases, nerve stimulation will be unsuccessful if the axon distance from the nanostructure exceeds 5µm. The temperature increase at a distance of 10µm from AuNHs in 5 ms is about 4.8 ° C, which is insufficient to generate AP. In addition, to study the current induced in the membrane, induced currents were calculated using a 6 and 3 ° C increase in temperature on the axon. Figure 3(D) shows that if the temperature increase doubles, the induced current to the membrane is quadrupled. These results confirm the potential of gold hexagonal nanoparticles for stimulation of neural fibers.

Biomedical Optics EXPRESS

3.3. Cardiac neural stimulation

Heart rhythm phases directly depend on heart muscle activity showing intracellular ion changes of heart cells. So an experimental animal study was done on the toad heart to explore the effects of AuNHs on heart rhythm. Three immature Eurasian green toads (weight 50-70 grams) were utilized and fixed horizontally. The use of anesthetics (such as ether and chloroform) disrupts the toad's regular cardiac rhythm. So no anesthesia was utilized in this trial. A continuous 532 nm laser with a 3 mm beam diameter and a power density of 100 $\frac{mW}{cm^2}$ irradiated AuNHs to increase their temperature. The laser was fixed at a distance of 5 cm from the top of the toad. First, the toad heart area was illuminated for 5 minutes just by laser. Then AuNHs were added and distributed on the heart area to determine the different effects of AuNHs heating and laser radiation. A two-dimensional nanoplasmonic structure was fixed on top of the heart area for heart activity recording. According to the required time for increasing the AuNHs temperature, the heart area was irradiated for more than 5 minutes. The experimental setup can be seen in Fig. 4(D). All animals participating in this study were cared for according to the ethics committee of Shahid Beheshti University, Iran.

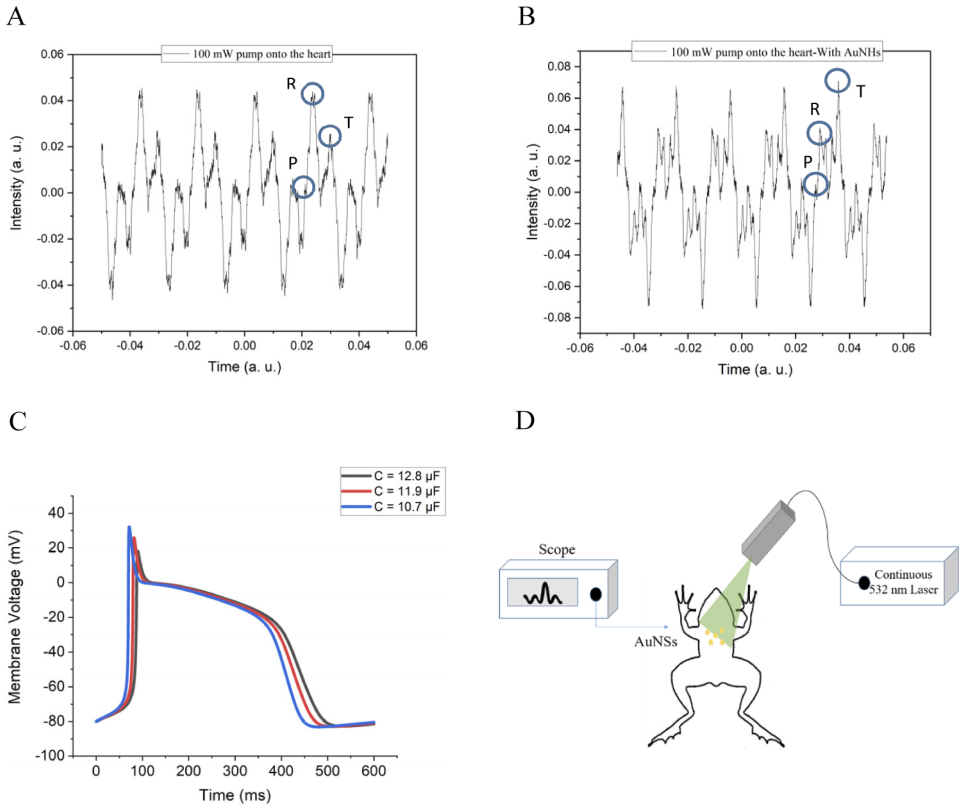

Fig. 4. **(A)** Toad heart rhythm with 532 nm laser irradiation. **(B)** Toad heart rhythm with gold nano hexagons under 532 nm irradiation on the toad heart area. **(C)** Change in membrane voltage of Purkinje fibers due to increased temperature. APD time is shortened as the temperature increases. (D) Experimental setup for toad heart stimulation.

Results of toad heart stimulation with AuNHs show significant changes in toad heart activity. Despite that laser irradiation without AuNHs had no significant effect on heart rhythm, irradiation of AuNH in the toad heart area affected heart rhythm. Figure 4(A) shows toad heart rhythm under laser with the wavelength of 532 nm irradiation that could not be seen any effect on its

Biomedical Optics EXPRESS

phases amplitude under the impression of laser radiation. T wave amplitude was impacted by an increase in temperature on the toad heart area owing to AuNHs photothermal effect, as illustrated in Fig. 4(B).

In comparison to toad heart rhythm before stimulation with AuNHs, T wave amplitude significantly has increased. T wave amplitude increase is due to some biological effects on the toad heart. For exploring these biological effects, cardiac action potential was simulated. According to the results published in Ref [36]., an increase in the temperature by prolonged irradiation of infrared laser reduces membrane capacity. Therefore, decreasing membrane capacity on cardiac AP shape was studied considering that temperature reduced the membrane capacity. For this purpose, membrane voltage adjustments were recorded by setting three different membrane capacities for the cardiac model. The initial membrane capacity of the model was 12.8 µF, but it was changed to 11.9 and 10.7 µF, and membrane voltage was recorded. Figure 4(C) shows that decreased membrane capacity reduces action potential duration (APD) time. When membrane capacity decreased to 11.9 and 10.7 µF, APD about 21 and 46 ms reduced, respectively. It has been shown that reducing APD time affects T wave amplitude [37,38]. There are a few reasons those are the cause of reducing AP durations. The first one is related to the increase in temperature and heating that in our work, our nano hexagons increased the temperature by almost 6 °C. It has been shown by Ref. [39] that increasing the temperature is effective in reducing the duration of AP. As a result, the amplitude of the T wave increases. So, probably, the heat effect of AuNHs is the first reason for increasing T wave amplitude. Increased intracellular calcium ion concentration is another factor that decreases APD [40]. It has been shown that temperature increase by IR laser led to an increase in intracellular free Ca^{2+} concentration in ventricular cardiomyocytes and cortical neurons [41,42]. It seems that photothermal effects of AuNHs affected intracellular Ca^{2+} concentration in the toad heart. In summary, our results show the effects of AuNHs photothermal on heart cells and cardiac activity. Moreover, this study can be considered as an early study for non-invasive optical pacing based on nanoparticles.

4. Conclusion

In this study, the photothermal effect of hexagonal gold nanoparticles such as absorption spectrum and the light-heat conversion rate were studied. Furthermore, cardiac and axonal action potentials were modeled, and the effects of thermal stimulation on them were investigated. The results showed that irradiation of AuNHs under continuous 532 nm laser led to about 6°C increase in temperature. In addition, it was shown that in this range of increase in temperature, gold nanohexagons could successfully stimulate small diameter axon fiber. Finally, thermal stimulation of the toad heart with AuNHs increased T wave amplitude on its heart rhythm. Changes in heart rhythm are probably related to increasing Ca^{2+} intracellular concentration due to the photothermal effect of hexagonal gold nanoparticles.

Appendix

A. Cardiac action potential

- Sodium current

$$I_{Na} = (g_{Na} - 140)(V - V_{Na}) \tag{9}$$

$$V_{Na} = \frac{RT}{zF} ln \frac{[Na^+]_o}{[Na^+]_i} \tag{10}$$

$$g_{Na} = x_{Na_{max}} m^3 h \tag{11}$$

- Chloride current

$$I_{Cl} = g_{Cl}(V - V_{Cl}) \tag{12}$$

Biomedical Optics EXPRESS

- Voltage and time-dependent potassium current:

$$I_{K1} = g_{K1}(V - V_{Na}) \tag{13}$$

$$g_{K1} = g_{k1_{max}} n^4 \tag{14}$$

- Voltage-dependent potassium current

$$I_{K2} = g_{K2}(V - V_{K2}) \tag{15}$$

$$V_{Na} = \frac{RT}{zF} ln \frac{[K^+]_o}{[K^+]_i} \tag{16}$$

R is the universal gas constant, T is the temperature, z is the number of elementary charges of the ion, and F is the Faraday constant. $[K^+]_o$ and, $[Na^+]_o$ are the extracellular concentration of potassium and sodium. $[K^+]_i$ and $[Na^+]_i$ are the intracellular concentration of potassium and sodium.

Table 1. Parameters used in the cardiac model

Parameter	Value
Resting potential	-80 (mV)
Cl Reversal Potential	-60 (mV)
Na Reversal Potential	35 (mV)
K Reversal Potential	-100 (mV)
$x_{Na max}$	0.4 (s/cm^2)
$g_{k1 max}$	1.2 (s/cm^2)
g_{Cl}	0.000075 (s/cm^2)
Initial membrane capacitance	12.8 μF
$[K^+]_i$	95 mM
$[K^+]_o$	2.5 mM
$[Na^+]_i$	7.5 mM
$[Na^+]_o$	111 mM

B. Axonal action potential

$$I_k = g_k(V - V_K), \tag{17}$$

$$I_{Na} = g_{Na}(V - V_{Na}), \tag{18}$$

$$I_l = g_l(V - V_l), \tag{19}$$

which g_k, g_{Na}, and g_l denote the conductivity of the potassium, sodium, and leakage currents, respectively. V_K, V_{Na}, and V_l are the reversal potentials of the potassium, sodium, and leakage channels.

Biomedical Optics EXPRESS

Table 2. Parameters used in the axonal model

Parameter	Value
Axon diameter	5 μm
Electrical current	4 nA
Resting potential	-65 (mV)
Leak Reversal Potential	-54 (mV)
Na Reversal Potential	50 (mV)
K Reversal Potential	-77(mV)
Na conductance x_2	0.12 (s/cm^2)
K conductance x_1	0.036 (s/cm^2)
Leak conductance x_3	0.003 (s/cm^2)
Axon Initial Temperature	21 °C
Initial membrane capacitance	1 μF
Q_{10}	$3^{\frac{(T-T_0)}{10}}$

Disclosures. The authors declare that there are no conflicts of interest related to this article.

Data availability. Data underlying the results presented in this paper are not publicly available at this time but may be obtained from the authors upon reasonable request.

References

1. M. A. El-Sayed, "Small is different: Shape-, size-, and composition-dependent properties of some colloidal semiconductor nanocrystals," Acc. Chem. Res. **37**(5), 326–333 (2004).
2. J. N. Anker, W. P. Hall, O. Lyandres, N. C. Shah, J. Zhao, and R. P. Van Duyne, "Biosensing with plasmonic nanosensors," Nat. Mater. **7**(6), 442–453 (2008).
3. R. Aroca, *Surface-Enhanced Vibrational Spectroscopy* (John Wiley and Sons, 2007).
4. D. Seo, C. P. Ji, and H. Song, "Polyhedral gold nanocrystals with Oh symmetry: From octahedra to cubes," J. Am. Chem. Soc. **128**(46), 14863–14870 (2006).
5. V. Bastys, I. Pastoriza-Santos, B. Rodíguez-González, R. Vaisnoras, and L. M. Liz-Marzán, "Formation of silver nanoprisms with surface plasmons at communication wavelengths," Adv. Funct. Mater. **16**(6), 766–773 (2006).
6. C. L. Nehl and J. H. Hafner, "Shape-dependent plasmon resonances of gold nanoparticles," J. Mater. Chem. **18**(21), 2415–2419 (2008).
7. M. Schütz, D. Steinigeweg, M. Salehi, K. Kömpe, and S. Schlücker, "Hydrophilically stabilized gold nanostars as SERS labels for tissue imaging of the tumor suppressor p63 by immuno-SERS microscopy," Chem. Commun. **47**(14), 4216–4218 (2011).
8. C. G. Khoury and T. Vo-Dinh, "Gold nanostars for surface-enhanced Raman scattering: synthesis, characterization and optimization," J. Phys. Chem. C **112**(48), 18849–18859 (2008).
9. C. Burda, X. Chen, R. Narayanan, and M. A. El-Sayed, "Chemistry and properties of nanocrystals of different shapes," Chem. Rev. **105**(4), 1025–1102 (2005).
10. A. Tomitaka, H. Arami, A. Ahmadivand, N. Pala, A. J. McGoron, Y. Takemura, M. Febo, and M. Nair, "Magneto-plasmonic nanostars for image-guided and NIR-triggered drug delivery," Sci. Rep. **10**(1), 10115 (2020).
11. J. Cury, L. Vande Perre, H. Smets, L. Stumpp, S. Vespa, A. Vanhoestenberghe, P. Doguet, J. Delbeke, R. El Tahry, S. P. Gorza, and A. Nonclercq, "Infrared neurostimulation in ex-vivo rat sciatic nerve using 1470 nm wavelength," J. Neural Eng. **18**(5), 056018 (2021).
12. J. M. Cayce, R. M. Friedman, G. Chen, E. D. Jansen, A. Mahadevan-Jansen, and A. W. Roe, "Infrared neural stimulation of primary visual cortex in non-human primates," NeuroImage **84**, 181–190 (2014).
13. X. Tan, I. Jahan, Y. Xu, S. Stock, C. C. Kwan, C. Soriano, X. Xiao, J. García-Añoveros, B. Fritzsch, and C. P. Richter, "Auditory neural activity in congenitally deaf mice induced by infrared neural stimulation," Sci. Rep. **8**(1), 388 (2018).
14. M. A. Ansari and V. V. Tuchin, "Infrared neurostimulation of earthworm: from modeling to experiment," Opt. Eng. **59**(06), 1 (2020).
15. M. W. Jenkins, A. R. Duke, S. Gu, Y. Doughman, H. J. Chiel, H. Fujioka, M. Watanabe, E. D. Jansen, and A. M. Rollins, "Optical pacing of the embryonic heart," Nat. Photonics **4**(9), 623–626 (2010).
16. M. W. Jenkins, Y. T. Wang, Y. Q. Doughman, M. Watanabe, Y. Cheng, and A. M. Rollins, "Optical pacing of the adult rabbit heart," Biomed. Opt. Express **4**(9), 1626 (2013).

Biomedical Optics EXPRESS

17. M. J. Alemzadeh-Ansari, M. A. Ansari, M. Zakeri, and M. Haghjoo, "Influence of radiant exposure and repetition rate in infrared neural stimulation with near-infrared lasers," Lasers Med. Sci. **34**(8), 1555–1566 (2019).
18. K. Eom, K. M. Byun, S. B. Jun, S. J. Kim, and J. Lee, "Theoretical Study on Gold-Nanorod-Enhanced Near-Infrared Neural Stimulation," Biophys. J. **115**(8), 1481–1497 (2018).
19. Z. Mou, M. You, and W. Xue, "Gold nanorod-assisted near-infrared stimulation of bullfrog sciatic nerve," Lasers Med. Sci. **33**(9), 1907–1912 (2018).
20. J. Yong, K. Needham, W. G. A. Brown, B. A. Nayagam, S. L. Mcarthur, A. Yu, and P. R. Stoddart, "Gold-nanorod-assisted near-infrared stimulation of primary auditory neurons," Adv. Healthc. Mater. **3**(11), 1862–1868 (2014).
21. C. Paviolo, A. C. Thompson, J. Yong, W. G. A. Brown, and P. R. Stoddart, "Nanoparticle-enhanced infrared neural stimulation," J. Neural Eng. **11**(6), 065002 (2014).
22. M. Q. Wang, N. Xia, X. Y. Wu, N. Hu, X. L. Zheng, and W. S. Hou, "980 nm infrared neural stimulation of sciatic nerve enhanced by carbon nanoparticles," in *International IEEE/EMBS Conference on Neural Engineering, NER* (IEEE Computer Society, 2017), pp. 215–218.
23. S. Saeidifard, F. Sohrabi, M. H. Ghazimoradi, S. M. Hamidi, S. Farivar, and M. A. Ansari, "Two-dimensional plasmonic biosensing platform: cellular activity detection under laser stimulation," J. Appl. Phys. **126**(10), 104701 (2019).
24. ÁC Horváth, S. Borbély, ÖC Boros, L. Komáromi, P. Koppa, P. Barthó, and Z. Fekete, "Infrared neural stimulation and inhibition using an implantable silicon photonic microdevice," Microsyst. Nanoeng. **6**(1), 1–12 (2020).
25. H. Kang, W. Hong, Y. An, S. Yoo, H. J. Kwon, and Y. Nam, "Thermoplasmonic optical fiber for localized neural stimulation," ACS Nano **14**(9), 11406–11419 (2020).
26. F. Hao, C. L. Nehl, J. H. Hafner, and P. Nordlander, "Plasmon resonances of a gold nanostar," Nano Lett. **7**(3), 729–732 (2007).
27. P. Strobbia, E. Languirand, and B. M. Cullum, "Recent advances in plasmonic nanostructures for sensing: a review," Opt. Eng. **54**(10), 100902 (2015).
28. T. K. Sau and C. J. Murphy, "Room temperature, high-yield synthesis of multiple shapes of gold nanoparticles in aqueous solution," J. Am. Chem. Soc. **126**(28), 8648–8649 (2004).
29. H. Richard Leuchtag, "Fit of the dielectric anomaly of squid axon membrane near heat-block temperature to the ferroelectric Curie-Weiss law," Biophys. Chem. **53**(3), 197–205 (1995).
30. S. Fribance, J. Wang, J. R. Roppolo, W. C. de Groat, and C. Tai, "Axonal model for temperature stimulation," J. Comput. Neurosci. **41**(2), 185–192 (2016).
31. Q. Liu, M. J. Frerck, H. A. Holman, E. M. Jorgensen, and R. D. Rabbitt, "Exciting cell membranes with a blustering heat shock," Biophys. J. **106**(8), 1570–1577 (2014).
32. D. Noble, "A modification of the Hodgkin—Huxley equations applicable to Purkinje fibre action and pacemaker potentials," J. Physiol. **160**(2), 317–352 (1962).
33. M. L. Hines and N. T. Carnevale, "The NEURON simulation environment," Neural Comput. **9**(6), 1179–1209 (1997).
34. P. R. Wiecha, "pyGDM—A python toolkit for full-field electro-dynamical simulations and evolutionary optimization of nanostructures," Comput. Phys. Commun. **233**, 167–192 (2018).
35. A. J. Saubermann and V. L. Scheid, "Elemental composition and water content of neuron and glial cells in the central nervous system of the North American medicinal leech (Macrobdella decora)," J. Neurochem. **44**(3), 825–834 (1985).
36. F. Kong, R. Jiao, K. Liu, X. Han, and C. Sun, "Continuous infrared laser irradiation decreased membrane capacitance of neuron cell," Proc. SPIE **11190**, 111901X (2019).
37. L. P. B. Meijs, L. Galeotti, E. P. Pueyo, D. Romero, R. B. Jennings, M. Ringborn, S. G. Warren, G. S. Wagner, and D. G. Strauss, "An electrocardiographic sign of ischemic preconditioning," Am. J. Physiol. - Hear. Circ. Physiol. **307**(1), H80–H87 (2014).
38. D. Di Bernardo, P. Langley, and A. Murray, "Effect of changes in heart rate and in action potential duration on the electrocardiogram T wave shape," Physiol. Meas. **23**(2), 355–364 (2002).
39. R. Coronel, J. M. T. de Bakker, F. J. G. Wilms-Schopman, T. Opthof, A. C. Linnenbank, C. N. Belterman, and M. J. Janse, "Monophasic action potentials and activation recovery intervals as measures of ventricular action potential duration: experimental evidence to resolve some controversies," Hear. Rhythm **3**(9), 1043–1050 (2006).
40. X. R. Fan, J. H. Ma, W. Wan, P. H. Zhang, C. Wang, and L. Wu, "Increased intracellular calcium concentration causes electrical turbulence in guinea pig ventricular myocytes," Sci. China: Life Sci. **54**(3), 240–247 (2011).
41. G. M. Dittami, S. M. Rajguru, R. A. Lasher, R. W. Hitchcock, and R. D. Rabbitt, "Intracellular calcium transients evoked by pulsed infrared radiation in neonatal cardiomyocytes," J. Physiol. **589**(6), 1295–1306 (2011).
42. A. Kaszas, G. Szalay, A. Slézia, A. Bojdán, I. Vanzetta, B. Hangya, B. Rózsa, R. O'Connor, and D. Moreau, "Two-photon GCaMP6f imaging of infrared neural stimulation evoked calcium signals in mouse cortical neurons in vivo," Sci. Rep. **11**(1), 9775 (2021).